

# Model Alignment Search

Satchel Grant<sup>1</sup>

## Abstract

When can we say that two neural systems are the same? The answer to this question is goal-dependent, and it is often addressed through correlative methods such as Representational Similarity Analysis (RSA) and Centered Kernel Alignment (CKA). We find ourselves chiefly interested in the relationship between representations and behavior, asking ourselves how we can isolate specific functional aspects of representational similarity to relate our measures to behavior—avoiding cause vs. correlation pitfalls in the process. In this work, we introduce Model Alignment Search (MAS), a method for causally exploring distributed representational similarity as it relates to behavior. The method learns invertible linear transformations that find an aligned subspace between two distributed networks’ representations where functional information can be isolated and manipulated. We first show that the method can be used to transfer values of specific causal variables—such as the number of items in a counting task—between networks with different training seeds and different architectures. We then explore open questions in number cognition by comparing different types of numeric representations in models trained on structurally different tasks, we explore differences between MAS and preexisting functional similarity methods, and lastly, we introduce a counterfactual latent auxiliary loss that helps shape functionally relevant alignments even in cases where we do not have causal access to one of the two models for training.

## 1. Introduction

An important question for understanding both Artificial and Biological Neural Networks (ANNs and BNNs) is know-

<sup>1</sup>Departments of Psychology and Computer Science, Stanford University, Stanford, USA. Correspondence to: Satchel Grant <grantsrb@stanford.edu>.

Preprint under review

ing what it means for one distributed system to model or represent another (Sucholutsky et al., 2023). Establishing isomorphisms between different distributed systems can be useful for simplifying their complexity and for understanding otherwise opaque inner mechanisms. We cannot yet measure from every individual neuron in most BNNs; even if we could, as is the case in ANNs, it is still difficult to find satisfying ways of understanding the neural behavior. Finding simplified models that exhibit the causal relationships of more complex distributed systems can make complex systems more interpretable and communicable, potentially leading to useful insights (Cao & Yamins, 2021; 2024; Richards et al., 2019). Furthermore, there are a number of open questions about how representations differ or converge across architectures, tasks, and modalities (Huh et al., 2024; Sucholutsky et al., 2023; Wang et al., 2024; Li et al., 2024; Hosseini et al., 2024; Zhang et al., 2024; Grant et al., 2024). Researchers often use correlational methods to measure the similarity of different neural representations. We can see examples of this in works that perform direct correlational analyses between individual ANN activations and BNN firing rates (Yamins & DiCarlo, 2016; Maheswaranathan et al., 2019; Khosla & Williams, 2023; Williams et al., 2022), and in works that use Representational Similarity Analysis (RSA)—or Centered Kernel Alignment (CKA) (Kornblith et al., 2019; Williams, 2024)—finding 2nd order isomorphisms between model and system (Kriegeskorte et al., 2008). We also see examples of this in linear decoding techniques, where linear decodability can be used as a metric for understanding the type of information encoded in distributed representations (Chen et al., 2020; Radford et al., 2021; Grill et al., 2020; Caron et al., 2021; Haxby et al., 2001; Haxby, 2013). A question remains, however, how to causally associate these similarity metrics with behavioral outcomes. Can we develop methods to understand functional representational alignment (Geiger et al., 2024; Cloos et al., 2024; Schaeffer et al., 2024)?

Some works have made progress toward understanding causal/functional representation similarity by transforming intermediate representations from one system into a usable form for another model. We see examples in works like Sexton & Love (2022) where they attempt to use transformed neural recordings in a trained computational model, and in *model stitching*, where a linear mapping is learned

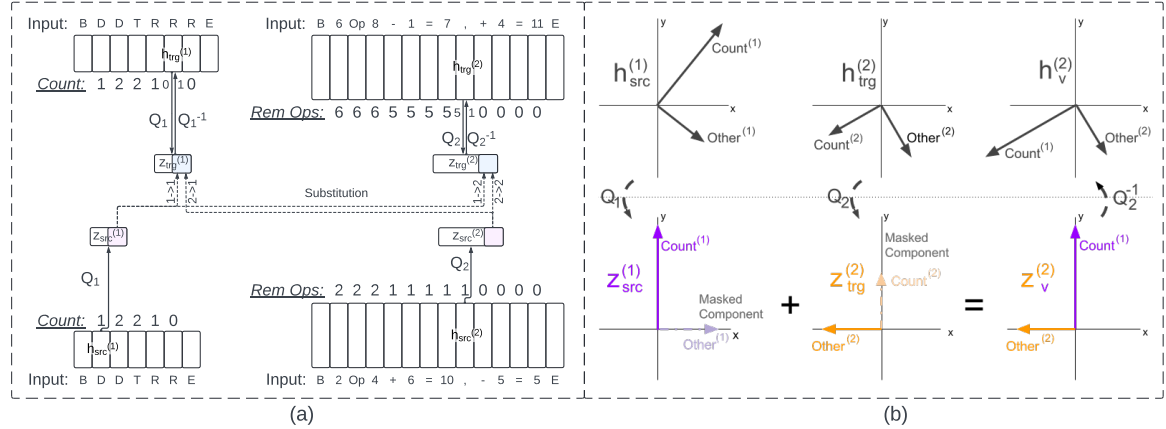


Figure 1: (a) Diagram of MAS showing all four possible intervention directions on the latent vectors (rectangles) of a Multi-Object Model<sub>1</sub> and an Arithmetic Model<sub>2</sub>. Each rectangle is a latent vector produced from the input token. The values of the intervened causal variables—Count for the Multi-Object and Rem Ops for the Arithmetic models—are replaced by the values of the causal variables from the source latents,  $h_{src}^{(i)}$ . The value of the variable before the intervention is displayed on the left side of the arrows underneath the target latents  $h_{trg}^{(i)}$ . The value after the intervention is shown on the right. The dotted *Substitution* arrows each correspond to a single causal intervention. The models make predictions using the intervened vector following the intervention. (b) A theoretic causal intervention that transfers the Count information from Model<sub>1</sub>'s latent representation,  $h_{src}^{(1)}$ , into Model<sub>2</sub>'s  $h_{trg}^{(2)}$ . The superscripts (1) and (2) refer to the originating model. The hidden state vectors,  $h_{src}^{(1)}$  and  $h_{trg}^{(2)}$ , are rotated into an aligned vector space using learned matrices  $Q_1$  and  $Q_2$ . In the aligned vectors,  $z_{src}^{(1)}$  and  $z_{trg}^{(2)}$ , the Count information lies along a disentangled component where it can be manipulated while preserving all other information. After the transfer, the rotated, intervened vector,  $z_{trg}^{(2,v)}$ , is returned to Model<sub>2</sub>'s hidden state space, using  $Q_2^{-1}$ . Model<sub>2</sub> can then use the intervened vector to continue making predictions.

from intermediate representations in one ANN to another for the purpose of measuring similarity or improving one of the two models (Lähner et al., 2023; Moschella et al., 2023; Bansal et al., 2021; Lenc & Vedaldi, 2015). To build upon these works, we ask: 1) what do these causal mappings tell us about the underlying representations of the two systems? Are behaviorally successful mappings both necessary and sufficient for claims of functional similarity? 2) How do we compare models with disparate behavioral outputs, and how can we isolate the similarity of specific functional information in the representations? And 3) How do we achieve causal relevance in systems that we do not have causal access—as is often the case in ANN to BNN comparisons?

In this work, we introduce Model Alignment Search (MAS) to measure functional similarity between distributed networks. MAS can be thought of as a multi-model extension of Distributed Alignment Search (DAS) (Geiger et al., 2021; 2023), a technique used to align ANNs to symbolic algorithms (or directed acyclic graphs). MAS learns a rotation matrix for each model with the goal of finding an aligned representational subspace where information can be causally interchanged between the models and within each individual model. These intervened representations are then returned

back to their original neural space where they can be used to produce behavior that can be compared to expected behavior.

We first validate MAS by comparing it to similarity measurements produced by RSA in multiple architectural and task variants. We then show how to use MAS even when one or both of the models use anti-Markovian states (Grant et al., 2024). We then show that MAS can reveal the representational similarity and dissimilarity in representations of number in models trained on structurally different tasks. We then show that MAS can be more restrictive than previous causal methods, like direct linear mappings (model stitching), and we provide a theoretical model to better understand desired restrictions. Lastly, we provide relevance to ANN-BNN comparisons by showing that we can introduce an auxiliary loss objective to recover causal relevance for causally inaccessible models. This loss function uses *counterfactual latent* vectors—latent vectors that match the desired representational makeup of the intervened vectors assuming a successful causal intervention—as training targets for the intervened vectors of the causally inaccessible model, thus constraining the alignment to be functionally relevant for the inaccessible system. We refer to this variant as Counterfactual latent MAS (CMAS).

The contributions of this work are as follows.

1. We introduce and validate MAS by comparing and contrasting to RSA.
2. We use MAS to causally explore representations of numbers across structurally different tasks.
3. We explore how MAS can improve upon previous causal similarity methods.
4. We introduce a *counterfactual latent* auxiliary loss objective that can be used to find causally relevant alignments in cases where one of the two models is causally inaccessible (making the technique relevant for comparisons between ANNs and BNNs).

## 2. Methods

In this work, we build upon the work of (Grant et al., 2024) to examine the causal similarity of distributed representations within models trained on next token prediction, numeric tasks. Each model is trained to > 99.99% accuracy on both training and validation data held before being analyzed and interpreted.

### 2.1. Numeric Equivalence Tasks

The goal of the numeric equivalence tasks is to reproduce a quantity of tokens that is initially observed at the start of the task. Each sequence consists of two phases: the demonstration (demo) and response phases. Each sequence has an associated *object quantity* that is uniformly sampled from 1 to 20. The ordering of the demo phase consists of a Beginning of sequence token, denoted B, a number of Demonstration (D) tokens equal in quantity to the object quantity, and a Trigger (T) token. The response phase then consists of the object quantity of Response (R) tokens and ends with the End of sequence (E) token. During the model training, we include all token types in the autoregressive, cross entropy loss, even though the number of D tokens and location of the T token is unpredictable from the sequence. A trial is considered correct when the model produces the appropriate number of R tokens followed by an E token during the response phase. We present two task variants:

**Multi-Object Task:** there are 3 possible demo token types  $\{D_a, D_b, D_c\}$  that are uniformly sampled at each D in the sequence. There is a single response token type, R. As an example of an object quantity of 2, the sequence could be: "B D<sub>c</sub> D<sub>a</sub> T R R E"

**Same-Object Task:** there is a single token type, C, that is used as both the demo token type and the response token type. An example of an object quantity of 2 would be: "B C C T C C E".

We make a change to the Multi-Object Task when training the transformer models to prevent them from learning a solution that relies on reading out positional information (Grant et al., 2024). In this task variant, each token in the demo phase has a 0.2 probability of being sampled as a unique "void" token type, V, that is irrelevant to the completion of the numeric equivalence task. An example sequence with an object count of 2 could be: "B V D V D T R R E". All evaluations use the original Multi-Object Task.

### 2.2. Arithmetic Task

We include an arithmetic task consisting of addition/subtraction operations, interlaced with the intermediate, cumulative value following each operation. An example sequence is as follows: "B 3 Op 4 + 3 = 7 , + 11 = 18 , - 5 = 13 E", where the numeral between B and Op indicates the number of operations in the sequence and the numeral following Op is a sampled starting value. The number of operations is uniformly sampled from 1-10. The starting value is uniformly sampled from 0-20. All numeric values are restricted to 0-20. The arithmetic operations are uniformly sampled from  $\{+, -\}$  when the cumulative value is in the range 1-19. Otherwise, the operation is selected to ensure the cumulative value stays in the range 0-20. The possible operands are uniformly sampled from the set that will restrict the subsequent cumulative value to the range 0-20. The sequence then displays the cumulative value after the "=" token. The "," token indicates that there are more operations in the sequence. The sequence ends with the E token after the originally indicated number of operations. We use a base 21 token system so that all values correspond to a single token.

### 2.3. Model Architectures

Each model in this work is autoregressively trained to perform only one of the tasks through next-token prediction (NTP). We train 2 model seeds for each task variant. We consider Gated Recurrent Units (GRUs) (Cho et al., 2014), Long-Short Term Memory recurrent networks (LSTMs) (Hochreiter & Schmidhuber, 1997), and two layer Transformers based on the Roformer architecture (Vaswani et al., 2017; Touvron et al., 2023; Su et al., 2023). The GRUs and Transformers use a dimensionality of 40, whereas the LSTM uses 20 dimensions for each the h and c vectors. We leave the details of GRU and LSTM cells to the referenced papers. The GRU and LSTM based models in this paper follow the structure:

$$h_{t+1} = f(h_t, x_t) \quad (1)$$

$$\hat{x}_{t+1} = g(h_{t+1}) \quad (2)$$

Where  $h_t$  is the hidden state vector at step  $t$ ,  $x_t$  is the input token at step  $t$ ,  $f$  is the recurrent function (either a GRU or LSTM cell), and  $g$  is a two layer (two matrix) feed-forward network (FFN) used to make a prediction,  $\hat{x}_{t+1}$ , of the token at step  $t+1$  from the updated hidden state  $h_{t+1}$ .

The transformer architecture uses Rotary Positional Encodings (RoPE) (Su et al., 2023) and GELU nonlinearities (Hendrycks & Gimpel, 2023). Transformers use a history of input tokens,  $X_t = [x_1, x_2, \dots, x_t]$ , at each time step,  $t$ , to make a prediction:  $\hat{x}_{t+1} = f(X_t)$ , where  $f$  is now the transformer architecture. We show results from 2 layer, single attention head transformers. We refer readers to Figure 6 for more details. See more training details in Appendix A.1.

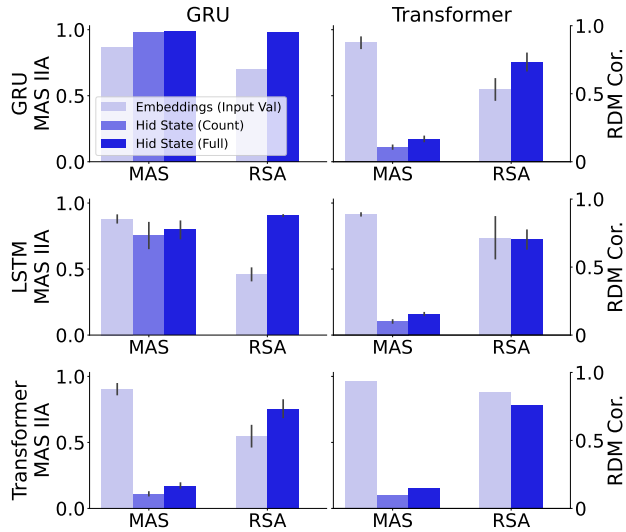


Figure 2: A performance comparison of MAS and RSA. The Model<sub>1</sub> architecture is consistent horizontally across panel rows. The Model<sub>2</sub> architecture is consistent vertically along the columns. All models are trained on the Multi-Object task. The bar colors correspond to different activation layers, and, in the case of MAS, the colors further distinguish which causal variables the analysis was conditioned upon. RDM Cor. is the value associated with an RSA whereas IIA is the intervention accuracy.

## 2.4. Model Alignment Search (MAS)

### 2.4.1. MAS FORMULATION

MAS can be thought of as a multi-model extension of DAS (Geiger et al., 2021; 2023), where both methods attempt to find a representational subspace for a given model that aligns with a Symbolic Algorithm (SA) (or directed acyclic graph), and MAS further measures the degree to which two models' SA aligned subspaces align with each other. MAS and DAS are interpretability methods that operate on NNs

with frozen weights. In our experiments, we first train the models to > 99% behavioral accuracy before freezing their weights. We note, however, that MAS can be used to align models with one another that are not fully trained. Refer to Figure 1 for a visual overview.

DAS tests the assumption that the hidden state,  $h^{(i)} \in R^{d_i}$ , for a single model<sub>i</sub> can be written as an orthogonal rotation  $h^{(i)} = Q_i z^{(i)}$ , where  $Q_i \in R^{d_i \times d_i}$  is a learned orthonormal matrix,  $z^{(i)} \in R^{d_i}$  consists of contiguous subspaces that encode high-level variables from SAs, and  $d_i$  is the size of the hidden state.

$$z^{(i)} = \begin{bmatrix} c_{\text{var}_1} \\ c_{\text{var}_2} \\ \vdots \\ c_{\text{var}_n} \end{bmatrix} \quad (3)$$

Where each  $c_{\text{var}_k} \in R^{d_{\text{var}_k}}$  is a column vector of length  $d_{\text{var}_k}$  satisfying the relation  $\sum_{k=1}^n d_{\text{var}_k} = d_i$ . The benefit of this alignment is that it allows us understand model<sub>i</sub>'s neural activity in terms of interpretable variables by allowing us to isolate and causally manipulate the value of each variable,  $\text{var}_k$  within the NN's latent representations. MAS builds on DAS by measuring the degree to which model<sub>1</sub> and model<sub>2</sub> share the same  $c_{\text{var}_k}$  for a given  $\text{var}_k$ . With this formulation, we can freely isolate and manipulate  $c_{\text{var}_k}$  encoded in  $h^{(i)}$  using a causal intervention:

$$h_v^{(i)} = Q_i((1 - D_{i,\text{var}_k})Q_i^{-1}h_{trg}^{(i)} + D_{j,\text{var}_k}Q_j^{-1}h_{src}^{(j)}) \quad (4)$$

Where  $i$  and  $j$  can take on either model index in the set of all models considered,  $Q_i$  is a scaled orthogonal rotation matrix for model<sub>i</sub>,  $D_{i,\text{var}_k} \in R^{d_i \times d_i}$  is a diagonal, binary matrix with  $d_{\text{var}_k}$  non-zero elements used to isolate the dimensions corresponding to  $c_{\text{var}_k}$ ,  $h_{src}^{(j)}$  is the *source vector* from which the subspace is harvested,  $h_{trg}^{(i)}$  is the *target vector* into which activity is substituted, and  $h_v^{(i)}$  is the resulting intervened vector that then replaces  $h_{trg}^{(i)}$  in the target model<sub>i</sub>'s processing, allowing the model to make causally intervened predictions. In this work, we train  $Q_i$  as the product  $s_i U_i$  where  $s_i$  is a learned scalar and  $U_i$  is an orthonormal matrix.

As an example, we can picture an SA where we assume that all behaviorally relevant information can be encoded in a single variable,  $c_{full}$ , and all extraneous, irrelevant information is encoded in a subspace  $c_{extra}$ . In this case,

$z^{(i)} = \begin{bmatrix} c_{full} \\ c_{extra}^{(i)} \end{bmatrix}$ , and we can freely isolate and intervene upon  $c_{full}$  using Equation 4 once we have learned each  $Q_i$  for each given  $D_{i,\text{full}}$ .

### 2.4.2. MAS TRAINING

MAS relies on the notion of counterfactual behavior to create intervention data to train and evaluate each  $Q_i$ . For a

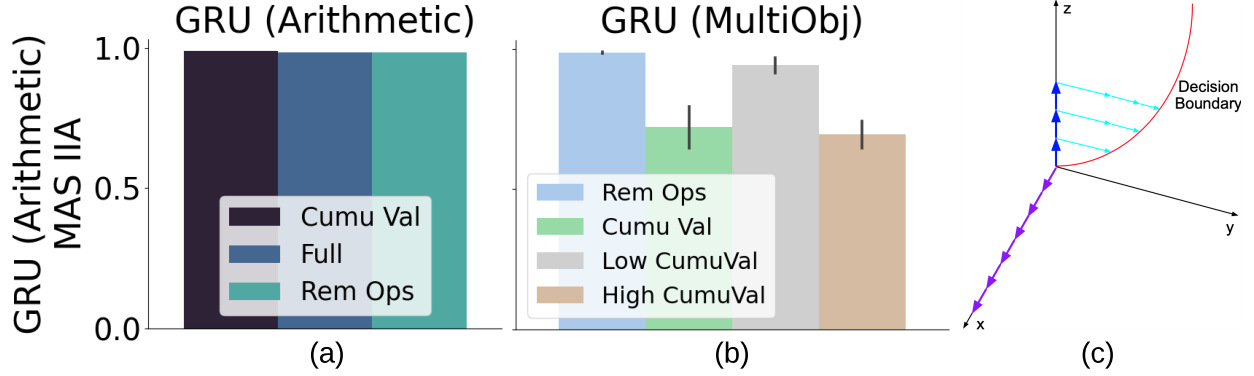


Figure 3: (a) MAS between GRUs trained on the Arithmetic task showing transferrability of the different types of information. (b) MAS used to compare the Count variable in the the Multi-Object GRUs to the Rem Ops and Cumu Val variables in the Arithmetic GRUs. Cumu Val results from MAS performed on all possible Cumu Val values. Low CumuVal results from a separate MAS analysis restricted to Cumu Val values in the range of the Rem Ops variable. High CumuVal results show a MAS analysis conditioned on values beyond the Rem Ops range. (c) Example trajectories of a theoretical model that provides a possible explanation for why Linear Map results can be inflated relative to MAS. See Section 3.4 for more details.

given SA, we know what the SA’s behavior will be after performing a causal intervention on one of its variables. The counterfactual behavior of the SA is the resulting behavior of the SA after changing a specific variable while keeping all other variables unchanged. This counterfactual behavior can be used as a training signal for  $Q_i$  using a standard Next-Token Prediction (NTP) autoregressive loss. It is possible for  $Q_i$  to equivalently learn any permutation of the subspaces in  $z_i$ , thus we can restrict our trainings to values of the diagonal matrices  $D_{i,\text{var}_k}$  that have contiguous, non-zero entries. It is then possible to treat  $d_{\text{var}_k}$  as a hyperparameter in independent trainings, selecting the  $Q_i$ - $D_{i,\text{var}_k}$  pair with the best results. Unless otherwise stated, we use values of  $d_{\text{var}}$  equal to 10, and we perform our causal interventions on individual time steps in the token sequences. We run the target model $_i$  up an independently sampled timestep  $t$  on the target sequence, using its latent representation at that point as the target vector,  $h_{t,\text{trg}}^{(i)}$ . We do the same on the source model $_j$  to obtain the source vector,  $h_{u,\text{src}}^{(j)}$ , at timestep  $u$  from a separate source sequence. We then construct  $h_{t,v}^{(i)}$  using Equation 4, and continue model $_i$ ’s predictions starting from time  $t$ , using  $h_{t,v}^{(i)}$  in place of  $h_{t,\text{trg}}^{(i)}$ . We perform batch gradient descent on  $Q_1$  and  $Q_2$  using the loss as follows for a single counterfactual sequence,  $k$ , of length  $S_k$  using  $i$  as the target model index and  $p_{\theta_i}(x_s)$  as the probability generated by model $_i$  for the counterfactual token label at step  $s$ :

$$\mathcal{L}_i^{(k)}(Q_i, Q_j) = -\frac{1}{S_k} \sum_{s=t}^{S_k} \log p_{\theta_i}(x_s^{(k)} | x_{<s}^{(k)}, h_{t,v}^{(k),(i)}) \quad (5)$$

$$\mathcal{L}_{\text{tot}} = \sum_{i=1}^2 \sum_{j=1}^2 \frac{1}{N} \sum_{k=1}^N \mathcal{L}_i^{(k)}(Q_i, Q_j) \quad (6)$$

Where  $N$  is the number of samples in the batch.

For the LSTM architecture, we perform MAS on a concatenation of the  $h$  and  $c$  recurrent state vectors (Hochreiter & Schmidhuber, 1997). In the GRUs, we operate on the recurrent hidden state. In the transformers, we operate on the residual stream following the first transformer layer (referred to as the Layer 1 Hidden States in Supplementary Figure 6) or the input embedding layer. We use 10000 intervention samples for training and 1000 samples for validation and testing. For all data, we uniformly sample trial object quantities, and unless otherwise stated, we uniformly sample intervention time points,  $t$  and  $u$ , from sequence positions containing demo tokens or response tokens (excluding BOS, trigger, and EOS tokens). We orthogonalize the rotation matrix using PyTorch’s orthogonal parameterization with default settings. We train  $Q$  with a batch size of 512 until convergence, selecting the checkpoint with the best validation performance for analysis. We use a learning rate of 0.003 and an Adam optimizer.

**MAS Evaluation:** Once the  $Q_1$  and  $Q_2$  training loss has converged, we can evaluate the quality of the alignment using the accuracy of each model’s predictions on counterfactual outputs from held out intervention data. We consider a trial correct when all deterministic tokens are predicted correctly using the argmax over logits. We report the proportion of trials correct for the worst performing causal intervention pairing,  $(i, j)$ , as the Interchange Intervention Accuracy (IIA).

#### 2.4.3. MAS VARIANTS

**Unidirectional MAS (UniMAS):** In some settings we wish to examine models for which we have neural recordings but

no causal access to the model (as is often the case in BNNs). We introduce a MAS variant called UniMAS that uses the activations from both models as source activations, but only uses model<sub>1</sub> as the target model during MAS trainings. Concretely, UniMAS changes Equation 6 to the following during trainings:

$$\mathcal{L}_{UniMAS} = \sum_{j=1}^2 \frac{1}{N} \sum_{k=1}^N \mathcal{L}_1^{(k)}(Q_1, Q_j) \quad (7)$$

As a baseline, we include **Linear Maps** which are trainings that exclusively use model 2 as the source model and model 1 as the target model,  $\mathcal{L}_{LinMaps} = \frac{1}{N} \sum_{k=1}^N \mathcal{L}_1^{(k)}(Q_1, Q_2)$ .

**Counterfactual latent MAS (CMAS):** We will show that the UniMAS trainings fail to learn an  $Q_2$  with strong IIA in the inaccessible model. To address this, we introduce an auxiliary loss function to the UniMAS trainings. The auxiliary objective relies on *Counterfactual Latent (CL) vectors*. We define CL vectors as latent vectors that encode the causal variables that we would expect to exist in the intervened vector,  $h_{trg,t}^{(i)}$  from Equation 4, after a successful causal intervention. We obtain these CL vectors from a neural representation dataset possessing situations and behaviors that are consistent with the information we wish to be encoded after the causal intervention. For example, if we have an SA with variables  $var_Y$ ,  $var_W$ , and  $var_{extra}$ , and following a causal intervention we expect  $h_{t,v}^{(2)}$  to have a value of  $y$  for variable  $var_Y$  and  $w$  for variable  $var_W$ , then the CL vector can be obtained from a pre-recorded representation  $h_{CL}^{(i)}$  where  $Q_i^{-1}h_{CL}^{(i)}$  has the same expected variable values:  $var_Y = y$  and  $var_W = w$ . The auxiliary loss  $\mathcal{X}^{(k)}$  for a single sample  $k$  is composed of an L2 loss and a cosine loss using CL vectors as the ground truth:

$$\mathcal{X}_{L2}^{(k)} = \frac{1}{2} \|h_{t,v}^{(k),(2)} - h_{CL}^{(k),(2)}\|_2^2 \quad (8)$$

$$\mathcal{X}_{cos}^{(k)} = -\frac{1}{2} \frac{h_{t,v}^{(k),(2)} \cdot h_{CL}^{(k),(2)}}{\|h_{t,v}^{(k),(2)}\|_2 \|h_{CL}^{(k),(2)}\|_2} \quad (9)$$

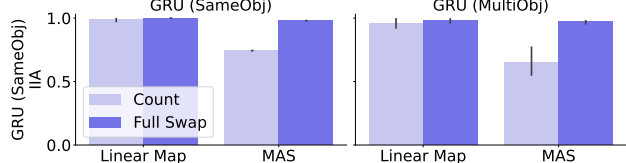


Figure 4: Performance comparison of MAS and direct linear mappings (Linear Map) between the Same-Object GRUs and between the Same-Object and Multi-Object GRUs. The Count information can be successfully transferred to and from Same-Object GRUs when using Linear Map but not in MAS.

where  $h_{t,v}^{(2)}$  is the intervened target vector for the causally inaccessible model, and  $k$  denotes the index of the sample within the batch. The total CMAS training loss is a weighted sum of the UniMAS autoregressive loss from Equation 7, and the auxiliary loss,  $\mathcal{L}_{CMAS} = \lambda(\mathcal{X}_{L2} + \mathcal{X}_{cos}) + (1 - \lambda)\mathcal{L}_{UniMAS}$  where  $\lambda$  is a hyperparameter.

As a baseline we include **Latent Fit** trainings which learn a single orthogonal matrix  $Q$  that maps  $h_{u,src}^{(k),(1)}$  to  $h_{CL}^{(k),(2)}$  minimizing only the  $\mathcal{X}_{L2}$  and/or  $\mathcal{X}_{cos}$ . We select  $\mathcal{X}_{L2}$  and/or  $\mathcal{X}_{cos}$  based on the best validation IIA.

## 2.5. Symbolic Algorithm Variables

The choice of the counterfactual behavior defines what SA variable(s) we can align the neural activity to using MAS. The simplest option is to align all behaviorally relevant information by simply using the exact behavior of the source model as the counterfactual behavior. This is similar to model stitching in previous works such as Bansal et al. (2021); Lenc & Vedaldi (2015); Sexton & Love (2022). In these cases of complete information transfer, MAS still differs from previous works in that it performs the interventions in multiple causal directions using  $Q_1$  and  $Q_2$ , and MAS isolates a functional subspace of the neural activity rather than using the entire latent space. MAS also has the ability to find alignments for specific types of information by conditioning the counterfactual sequences specific causal variables (i.e. the count of the sequence in the numeric equivalence tasks).

In all numeric equivalence tasks, we prevent interventions on representations resulting from the BOS, T, and EOS tokens. In the arithmetic task, we only perform interventions on representations after the "," token. We perform MAS using each of the following causal variables, where the corresponding task is denoted in parentheses:

1. **Full** (Arithmetic/Num Equivalence): Refers to cases in which we transfer all causally relevant information between models (not all activations).
2. **Count** (Num Equivalence): The difference between the number of observed demo tokens and the number of response tokens in the sequence. Example: the following sequences have a Count of 2 at the last token: "B D D" ; "B D D D T R"
3. **Last Value** (Num Equivalence): The value of the input token with respect to changing the Count of the sequence. We assign the values as D=1, R=-1, and all other tokens are 0. Example: if we change the Last Value of a single D token from 1 to -1, the counterfactual sequence should be "B D D D T R E". Example: in a partial sequence "B D D T R", changing the R token from -1 to 1 results in: "B D D T R R R E".

4. **Cumu Val** (Arithmetic): The cumulative value of the arithmetic sequence in the Arithmetic task. Example: if we substitute in a value of 3 at the “,” token in the sequence “B 2 Op 3 + 5 = 8 ,” the counterfactual sequence could be “B 2 Op 3 + 5 = 8 , + 2 = 5 E” where the “+” and “2” are provided by the task.
5. **Rem Ops** (Arithmetic): The remaining number of operations in the arithmetic sequence. Example: we substitute in a value of 1 at the “,” token in the sequence “B 3 Op 3 + 5 = 8 ,” the counterfactual sequence could be “B 3 Op 3 + 5 = 8 , + 1 = 9 E” where the “+” and “1” are provided.

## 2.6. Additional Methods

**Representational Similarity Analysis (RSA):** For a given model layer, we run the model on a batch of sequences consisting of 15 sequences from each object quantity 1-20. We then sample 1000 representational vectors uniformly from all time points excluding padding and end of sequence tokens. We construct a Representational Dissimilarity Matrix (RDM) as 1 minus the cosine similarity matrix over each pair-wise comparison of the representations (resulting in an RDM of dimensions  $1000 \times 1000$ ). We create an RDM for two models and compare the RDMs using Spearman’s rank correlation on the lower triangle of each matrix (Virtanen et al., 2020). We perform the RDM sampling 10 times and report the average over all 10 correlations.

## 3. Results/Discussion

### 3.1. MAS

We first turn our attention to the MAS IIA in Figure 2. The figure shows analyses where Model<sub>1</sub> is consistent horizontally across each row and Model<sub>2</sub> is displayed vertically along each column. We exclude comparisons of each model seed with itself. We see the MAS results conditioned on three different variables: Full, Count, and Last Value (see Section 2.5). The IIA shows the proportion of trials with successful counterfactual behavior after the causal interventions. A trial is considered successful if all deterministic counterfactual tokens are predicted correctly. For the Full and Count variables, causal interventions are performed on the hidden state vector after the recurrent processing in recurrent models and on the hidden states following the first transformer layer in transformers. Causal interventions conditioned on the Last Value variable are performed on the input embedding layer in all architectures.

We see from Figure 2 and Appendix 7 that MAS is successful at performing the Full variable interventions between different recurrent model seeds. This is consistent with the findings of previous work on direct linear mappings between networks (Lenc & Vedaldi, 2015; Bansal et al., 2021; Lähner

et al., 2023; Sexton & Love, 2022; Sucholutsky et al., 2023). Furthermore, MAS is successful at transferring the Count between the Multi-Object GRUs that have previously been shown to have an interchangeable Count variable using DAS (Grant et al., 2024). This success is qualified by MAS’ inability to transfer the Count when one of the two models is a Same-Object GRU (Figure 4), which is also expected from DAS. MAS on the hidden states of the transformers is largely unsuccessful with a value of 0.087, whereas MAS on the embeddings is successful with a value of 0.961. This is consistent with previous work that has shown the transformers solve the numeric equivalence tasks without encoding a Markovian cumulative state. Instead, they rely on re-solving the task at each step in the sequence (Grant et al., 2024; Behrens et al., 2024). See Figure 7 for DAS results.

### 3.2. MAS vs RSA

RSA is a second order correlational method that examines the similarity between sample correlation matrices constructed from two models’ representations (see Appendix A.3 for details). We provide comparisons between models differing only by seed to establish an upper limit on MAS and RSA values. We also provide GRU-LSTM comparisons to establish value changes resulting from architectural differences. Turning to Figure 2 and Appendix 7, we highlight that RSA provides a lower value than MAS on the embedding layers and a larger value than MAS on the the hidden states of the transformers. In the case of the hidden states in the Transformer-Transformer comparison (the lower rightmost panel), we see an RSA value of 0.78 and a CKA value of 0.96 in the appendix. The values in this comparison are difficult to interpret, as we might expect higher values due to similarities in architecture and training, but we also know from causal experiments that there is little causal transferrability between the transformers’ representations. We note that questions on how to interpret RSA values have been addressed in previous works (Kriegeskorte et al., 2008; Sucholutsky et al., 2023; Dujmović et al., 2022).

### 3.3. Arithmetic

We include a MAS analysis between Arithmetic GRUs and GRUs trained on the Numeric Equivalence tasks (see Figure 3). The leftmost panel shows that we can successfully align the Cumu Val, and the Rem Ops variables between and within the Arithmetic GRUs. The middle panel shows that MAS can successfully align the Count with the Rem Ops variables between GRUs trained on the Multi-Object and Arithmetic tasks respectively. These results are qualified by the lower IIA alignment between the Count and the Cumu Val variables. We see that when we perform MAS only on Cumu Val values that are shared with possible the Rem Ops values (Low CumuVal), the results are much higher but still do not match the results from Rem Ops. Thes findings are

consistent with the hypothesis that these GRUs are using different types of numeric representations for arithmetic than incremental counting.

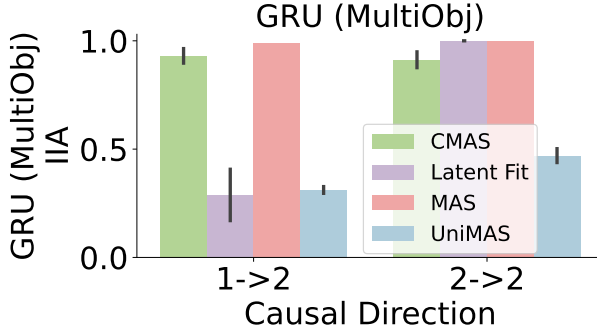


Figure 5: The IIA in the causally untrained directions for CMAS on the Multi-Object GRU models on the Full variable. The x labels denote the intervention directions where “1” and “2” denote the model index and the arrow points from the source to the target model. Latent Fit variants fit a transformation to the latent vectors in one direction without including causal behavior training. UniMAS and MAS show a lower and upper bound on CMAS performance. The  $2 \rightarrow 2$  Latent Fit direction is trivial.

### 3.4. Direct Linear Mappings

Turning to Figure 4, we compare the IIA of MAS to direct linear mappings (denoted Linear Map). The Linear Map trainings are equivalent to MAS trained in a single causal direction with the IIA reported from only that trained causal direction. We see that the Count variable can be successfully transferred between the Same-Object GRUs when using direct linear mappings. This is in contrast to MAS and the results of DAS from previous work (Grant et al., 2024). We introduce a theoretical model in Figure 3 as a possible explanation.

Turning to Figure 3, we see three components of a theoretical models’ state vector and their corresponding values at different points along 3 different trajectories. Each trajectory begins at the 0,0,0 coordinate. Each dark blue arrow represents an increment in the number of demo tokens, allowing the total number of demo tokens to be represented as the magnitude of the z-component. The number of response tokens is encoded along the y-axis, and the red curve represents the model’s decision boundary for outputting the E token. For a single trajectory, this model effectively counts up along the z-axis, then counts along the y-axis, and finishes when it has reached the non-linear decision boundary. Along the x-axis, we show a vector component that does not affect the model’s functional solution to the task, but still encodes relevant information. In this model, it is possible

to linearly decode the Count using the difference between twice the magnitude of the z-component and the magnitude of the x-component. More precisely,  $\text{Count} = 2z - x$ . It is possible to then map this information to the equivalent of the z-axis in a similar target model while discarding its y-component. This target model could then continue counting demo tokens or begin counting response tokens depending on its phase. It is important to note that this substitution is likely only possible if the mapping can push all conflicting causally relevant information into the null space of the target model; remnants of the z or y components could interfere with the counterfactual behavior. This effect is only a potential explanation for why the IIA observed in MAS is lower. Namely, the within model MAS interventions could prevent solutions that “throw away” residual information. We do not make efforts to prove that this theoretical model accounts for the results we see in Figure 4, it only serves as a *potential* explanation for the results.

### 3.5. CMAS

We can see from Figure 5 the results of CMAS compared to MAS, UniMAS, and Latent Fits. It is important to note that the Latent Fit, UniMAS, and CMAS variants do not include the autoregressive counterfactual training signal in causal directions  $1 \rightarrow 2$  and  $2 \rightarrow 2$ . MAS provides a theoretic upper bound on the possible IIA for CMAS. UniMAS provides a lower bound on the possible CMAS performance. We also note that the UniMAS results demonstrate that the causally relevant  $\mathcal{R}_2^{-1}$  is not automatically learned. Lastly, Latent Fit—which trains a rotation matrix to map latent vectors from  $\text{Model}_1$  to latent vectors of  $\text{Model}_2$  without any causal behavioral training—provides a baseline of existing methods. We see that CMAS recovers much of the possible performance of MAS whereas the Latent Fit performs near the lower bound. This demonstrates the potential of CMAS to recover causally relevant intervention rotation matrices even when we do not have causal access to one of the models in the comparison.

## 4. Limitations/Future Directions

We highlight that our results demonstrate the possibility to learn alignments that are functionally relevant in only one causal direction. Although MAS does not guarantee isolation and alignment of only functionally relevant information, it is more restrictive than existing methods while allowing for the desired alignment of functional information. Future MAS explorations can narrow the focus on functional information by finding the minimum transferrable subspace.

Despite CMAS’s successes, we are aware of the difficulty of evaluating the causal relevance of the interventions without causal access to the inaccessible model. We note, however, that CMAS still may provide value in biological settings

as the method can potentially remove the need for BNN counterfactual behavioral training data by using a brute-force approach of multiple independent CMAS trainings that can then be evaluated for causal relevance.

## Acknowledgments

Thank you to the PDP Lab and the Stanford Psychology department for funding. Thank you to Stephen Baccus, Noah Goodman, Zen Wu, Atticus Geiger, Linas Nasvytis, Jenelle Feather, Chris Potts, Alexa Tartaglini, Daniel Wuragaft, the PDP lab, and the Stanford Mech Interp community for thoughtful discussion. Thanks to Joshua Melander, Josh Wilson, Ben Prystawski, Jerome Han, and Andrew Lampinen for thoughtful discussion and paper feedback. Special thanks to Jay McClelland for encouragement, paper feedback, and many thoughtful conversations.

## Impact Statement

This paper presents work whose goal is to advance the field of Machine Learning, Cognitive Science, and Systems Neuroscience. There are many potential societal consequences of this work, none which we feel must be specifically highlighted here.

## References

Ba, J. L., Kiros, J. R., and Hinton, G. E. Layer normalization, 2016. URL <https://arxiv.org/abs/1607.06450>.

Bansal, Y., Nakkiran, P., and Barak, B. Revisiting Model Stitching to Compare Neural Representations, June 2021. URL <https://arxiv.org/abs/2106.07682>. arXiv:2106.07682 [cs, stat].

Behrens, F., Biggio, L., and Zdeborová, L. Counting in small transformers: The delicate interplay between attention and feed-forward layers, 2024. URL <https://arxiv.org/abs/2407.11542>.

Cao, R. and Yamins, D. Explanatory models in neuroscience: Part 1 – taking mechanistic abstraction seriously, April 2021. URL <https://arxiv.org/abs/2104.01490>. arXiv:2104.01490 [cs, q-bio].

Cao, R. and Yamins, D. Explanatory models in neuroscience, Part 2: Functional intelligibility and the contravariance principle. *Cognitive Systems Research*, 85:101200, June 2024. ISSN 1389-0417. doi: 10.1016/j.cogsys.2023.101200. URL <https://www.sciencedirect.com/science/article/pii/S1389041723001341>.

Caron, M., Touvron, H., Misra, I., Jégou, H., Mairal, J., Bojanowski, P., and Joulin, A. Emerging properties in self-supervised vision transformers, 2021.

Chen, T., Kornblith, S., Norouzi, M., and Hinton, G. A simple framework for contrastive learning of visual representations. 2020.

Cho, K., van Merriënboer, B., Gülcühre, Ç., Bougares, F., Schwenk, H., and Bengio, Y. Learning phrase representations using RNN encoder-decoder for statistical machine translation. *CoRR*, abs/1406.1078, 2014. URL <http://arxiv.org/abs/1406.1078>.

Cloos, N., Li, M., Siegel, M., Brincat, S. L., Miller, E. K., Yang, G. R., and Cueva, C. J. Differentiable optimization of similarity scores between models and brains, 2024. URL <https://arxiv.org/abs/2407.07059>.

Dujmović, M., Bowers, J. S., Adolfi, F., and Malhotra, G. The pitfalls of measuring representational similarity using representational similarity analysis. *bioRxiv*, 2022. doi: 10.1101/2022.04.05.487135. URL <https://www.biorxiv.org/content/early/2022/04/07/2022.04.05.487135>.

Geiger, A., Lu, H., Icard, T., and Potts, C. Causal abstractions of neural networks. *CoRR*, abs/2106.02997, 2021. URL <https://arxiv.org/abs/2106.02997>.

Geiger, A., Wu, Z., Potts, C., Icard, T., and Goodman, N. D. Finding alignments between interpretable causal variables and distributed neural representations, 2023.

Geiger, A., Ibeling, D., Zur, A., Chaudhary, M., Chauhan, S., Huang, J., Arora, A., Wu, Z., Goodman, N., Potts, C., and Icard, T. Causal abstraction: A theoretical foundation for mechanistic interpretability, 2024. URL <https://arxiv.org/abs/2301.04709>.

Grant, S., Goodman, N. D., and McClelland, J. L. Emergent symbol-like number variables in artificial neural networks, 2024.

Grill, J.-B., Strub, F., Altché, F., Tallec, C., Richemond, P. H., Buchatskaya, E., Doersch, C., Pires, B. A., Guo, Z. D., Azar, M. G., Piot, B., Kavukcuoglu, K., Munos, R., and Valko, M. Bootstrap your own latent: A new approach to self-supervised learning, 2020.

Haxby, J. V. Multivariate pattern analysis of fMRI: Parcellating abstract from concrete representations. *NEuroimage*, 62(2):2013, 2013. doi: 10.1016/j.neuroimage.2012.03.016.Multivariate.

Haxby, J. V., Gobbini, M. I., Furey, M. L., Ishai, A., Schouten, J. L., and Pietrini, P. Distributed and overlapping representations of faces and objects in ventral temporal cortex. *Social Neuroscience: Key Readings*, 293 (September):87–96, 2001. doi: 10.4324/9780203496190.

Hendrycks, D. and Gimpel, K. Gaussian error linear units (gelus), 2023. URL <https://arxiv.org/abs/1606.08415>.

Hochreiter, S. and Schmidhuber, J. Long short-term memory. *Neural Computation*, 9(8):1735–1780, 11 1997. ISSN 0899-7667. doi: 10.1162/neco.1997.9.8.1735. URL <https://doi.org/10.1162/neco.1997.9.8.1735>.

Hosseini, E., Casto, C., Zaslavsky, N., Conwell, C., Richardson, M., and Fedorenko, E. Universality of representation in biological and artificial neural networks. *bioRxiv*, 2024. doi: 10.1101/2024.12.26.629294. URL <https://www.biorxiv.org/content/early/2024/12/26/2024.12.26.629294>.

Huh, M., Cheung, B., Wang, T., and Isola, P. The platonic representation hypothesis, 2024. URL <https://arxiv.org/abs/2405.07987>.

Khosla, M. and Williams, A. H. Soft matching distance: A metric on neural representations that captures single-neuron tuning, 2023. URL <https://arxiv.org/abs/2311.09466>.

Kornblith, S., Norouzi, M., Lee, H., and Hinton, G. Similarity of neural network representations revisited, 2019. URL <https://arxiv.org/abs/1905.00414>.

Kriegeskorte, N., Mur, M., and Bandettini, P. Representational similarity analysis - connecting the branches of systems neuroscience. *Frontiers in Systems Neuroscience*, 2, 2008. ISSN 1662-5137. doi: 10.3389/neuro.06.004.2008. URL <https://www.frontiersin.org/articles/10.3389/neuro.06.004.2008>.

Lenc, K. and Vedaldi, A. Understanding image representations by measuring their equivariance and equivalence, 2015. URL <https://arxiv.org/abs/1411.5908>.

Li, J., Kementchedjhieva, Y., Fierro, C., and Søgaard, A. Do Vision and Language Models Share Concepts? A Vector Space Alignment Study. *Transactions of the Association for Computational Linguistics*, 12:1232–1249, September 2024. ISSN 2307-387X. doi: 10.1162/tacl\_a\_00698. URL [https://doi.org/10.1162/tacl\\_a\\_00698](https://doi.org/10.1162/tacl_a_00698).

Lähner, Z., Moeller, M., Fumero, M., Rodolà, E., Domine, C., Locatello, F., Dziugaite, K., and Caron, M. On the Direct Alignment of Latent Spaces. 2023.

Maheswaranathan, N., McIntosh, L. T., Tanaka, H., Grant, S., Kastner, D. B., Melander, J. B., Nayebi, A., Brezovec, L., Wang, J., Ganguli, S., and Baccus, S. A. The dynamic neural code of the retina for natural scenes. *bioRxiv*, 2019. doi: 10.1101/340943. URL <https://www.biorxiv.org/content/early/2019/12/17/340943>.

Moschella, L., Maiorca, V., Fumero, M., Norelli, A., Locatello, F., and Rodolà, E. Relative representations enable zero-shot latent space communication, March 2023. URL <http://arxiv.org/abs/2209.15430>. arXiv:2209.15430 [cs].

Paszke, A., Gross, S., Massa, F., Lerer, A., Bradbury, J., Chanan, G., Killeen, T., Lin, Z., Gimelshein, N., Antiga, L., Desmaison, A., Kopf, A., Yang, E. Z., DeVito, Z., Raison, M., Tejani, A., Chilamkurthy, S., Steiner, B., Fang, L., Bai, J., and Chintala, S. Pytorch: An imperative style, high-performance deep learning library. *CoRR*, abs/1912.01703, 2019. URL <http://arxiv.org/abs/1912.01703>.

Radford, A., Kim, J. W., Hallacy, C., Ramesh, A., Goh, G., Agarwal, S., Sastry, G., Askell, A., Mishkin, P., Clark, J., Krueger, G., and Sutskever, I. Learning transferable visual models from natural language supervision, 2021.

Richards, B. A., Lillicrap, T. P., Beaudoin, P., Bengio, Y., Bogacz, R., Christensen, A., Clopath, C., Costa, R. P., de Berker, A., Ganguli, S., Gillon, C. J., Hafner, D., Kepecs, A., Kriegeskorte, N., Latham, P., Lindsay, G. W., Miller, K. D., Naud, R., Pack, C. C., Poirazi, P., Roelfsema, P., Sacramento, J., Saxe, A., Scellier, B., Schapiro, A. C., Senn, W., Wayne, G., Yamins, D., Zenke, F., Zylberberg, J., Therien, D., and Kording, K. P. A deep learning framework for neuroscience. *Nature Neuroscience*, 22(11):1761–1770, November 2019. ISSN 1546-1726. doi: 10.1038/s41593-019-0520-2. URL <https://www.nature.com/articles/s41593-019-0520-2>. Publisher: Nature Publishing Group.

Schaeffer, R., Khona, M., Chandra, S., Ostrow, M., Miranda, B., and Koyejo, S. Does maximizing neural regression scores teach us about the brain? In *UniReps: 2nd Edition of the Workshop on Unifying Representations in Neural Models*, 2024. URL <https://openreview.net/forum?id=vbtj05J68r>.

Sexton, N. J. and Love, B. C. Reassessing hierarchical correspondences between brain and deep networks through direct interface. *Science Advances*, 8(28):eabm2219, July 2022. doi: 10.1126/sciadv.abm2219. URL <https://www.science.org/doi/10.1126/sciadv.abm2219>. Publisher: American Association for the Advancement of Science.

Su, J., Lu, Y., Pan, S., Murtadha, A., Wen, B., and Liu, Y. Roformer: Enhanced transformer with rotary position embedding, 2023.

Sucholutsky, I., Muttenhaler, L., Weller, A., Peng, A., Bobu, A., Kim, B., Love, B. C., Grant, E., Groen, I., Achterberg,

J., Tenenbaum, J. B., Collins, K. M., Hermann, K. L., Oktar, K., Greff, K., Hebart, M. N., Jacoby, N., Zhang, Q., Marjeh, R., Geirhos, R., Chen, S., Kornblith, S., Rane, S., Konkle, T., O'Connell, T. P., Unterthiner, T., Lampinen, A. K., Müller, K.-R., Toneva, M., and Griffiths, T. L. Getting aligned on representational alignment, 2023. URL <https://arxiv.org/abs/2310.13018>.

Touvron, H., Lavril, T., Izacard, G., Martinet, X., Lachaux, M.-A., Lacroix, T., Rozière, B., Goyal, N., Hambro, E., Azhar, F., Rodriguez, A., Joulin, A., Grave, E., and Lample, G. Llama: Open and efficient foundation language models, 2023.

Vaswani, A., Shazeer, N., Parmar, N., Uszkoreit, J., Jones, L., Gomez, A. N., Kaiser, L., and Polosukhin, I. Attention is all you need. *CoRR*, abs/1706.03762, 2017. URL <http://arxiv.org/abs/1706.03762>.

Virtanen, P., Gommers, R., Oliphant, T. E., Haberland, M., Reddy, T., Cournapeau, D., Burovski, E., Peterson, P., Weckesser, W., Bright, J., van der Walt, S. J., Brett, M., Wilson, J., Millman, K. J., Mayorov, N., Nelson, A. R. J., Jones, E., Kern, R., Larson, E., Carey, C. J., Polat, İ., Feng, Y., Moore, E. W., VanderPlas, J., Laxalde, D., Perktold, J., Cimrman, R., Henriksen, I., Quintero, E. A., Harris, C. R., Archibald, A. M., Ribeiro, A. H., Pedregosa, F., van Mulbregt, P., and SciPy 1.0 Contributors. SciPy 1.0: Fundamental Algorithms for Scientific Computing in Python. *Nature Methods*, 17:261–272, 2020. doi: 10.1038/s41592-019-0686-2.

Wang, J., Ge, X., Shu, W., Tang, Q., Zhou, Y., He, Z., and Qiu, X. Towards Universality: Studying Mechanistic Similarity Across Language Model Architectures, October 2024. URL <http://arxiv.org/abs/2410.06672>. arXiv:2410.06672 [cs].

Williams, A. H. Equivalence between representational similarity analysis, centered kernel alignment, and canonical correlations analysis. *bioRxiv*, 2024. doi: 10.1101/2024.10.23.619871. URL <https://www.biorxiv.org/content/early/2024/10/24/2024.10.23.619871>.

Williams, A. H., Kunz, E., Kornblith, S., and Linderman, S. W. Generalized shape metrics on neural representations, 2022. URL <https://arxiv.org/abs/2110.14739>.

Yamins, D. L. and DiCarlo, J. J. Using goal-driven deep learning models to understand sensory cortex. *Nature Neuroscience*, 19(3):356–365, 2016. ISSN 15461726. doi: 10.1038/nn.4244.

Zar, J. H. Spearman rank correlation. *Encyclopedia of Biostatistics*, 7, 2005.

Zhang, L., Yang, Q., and Agrawal, A. Assessing and learning alignment of unimodal vision and language models, 2024. URL <https://arxiv.org/abs/2412.04616>.

## A. Appendix / Supplementary material

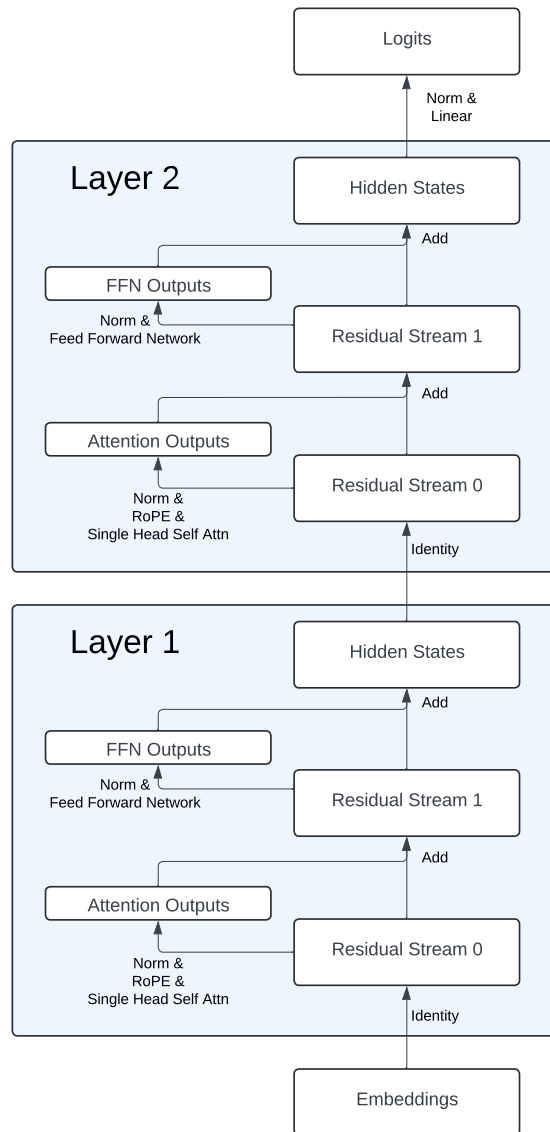


Figure 6: Figure and caption taken from Grant et al. (2024). Diagram of the transformer architecture used in this work. White rectangles represent activation vectors, arrows represent functional operations. All causal interventions were performed on either the Hidden State activations from Layer 1 or the Embeddings layer. All normalizations are Layer Norms (Ba et al., 2016).

### Model Alignment Search

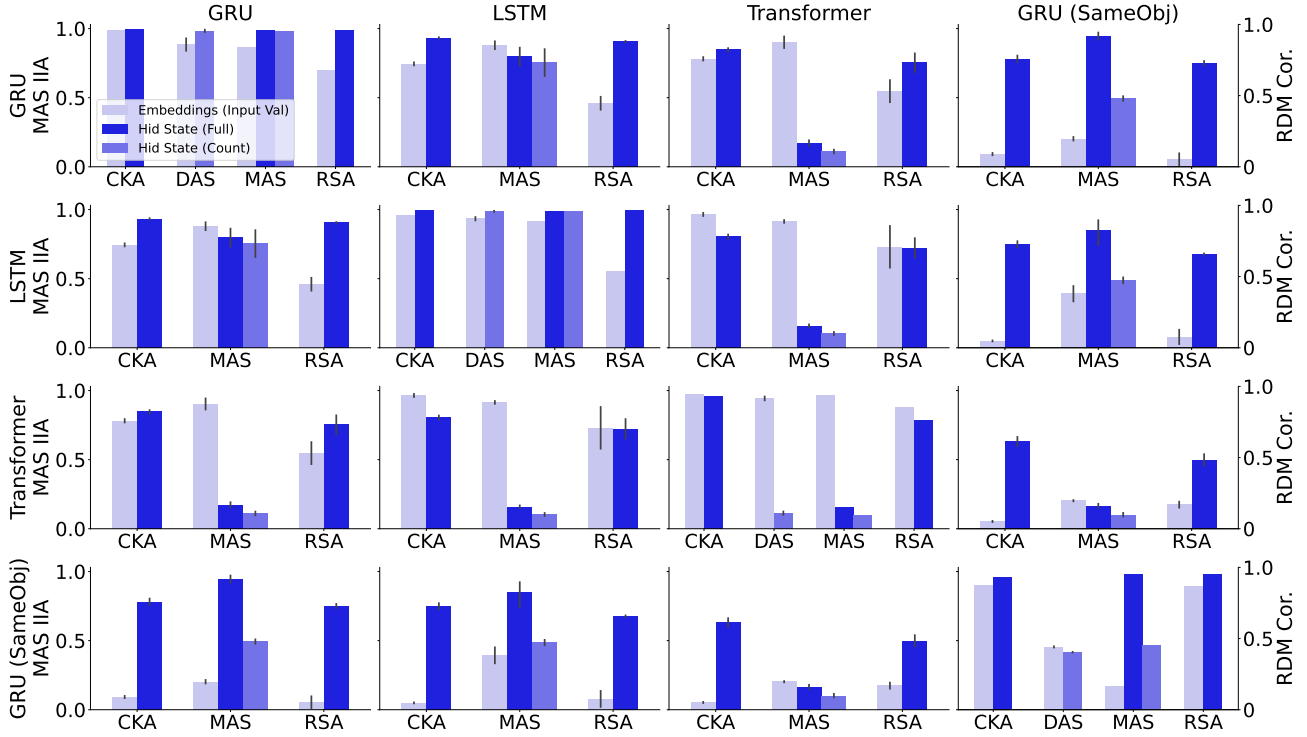


Figure 7: A performance comparison of MAS against RSA. The rows of panels show Model 1 whereas the columns represent the Model 2 in the context of the MAS diagram Figure 1. The different colors represent different activation layers within the models, and, in the case of MAS, the colors further distinguish which causal variables the analysis was conditioned upon. Results from DAS and CKA. DAS can only be applied within individual model seeds.

#### A.1. Model Details

All artificial neural network models were implemented and trained using PyTorch (Paszke et al., 2019) on Nvidia Titan X GPUs. Unless otherwise stated, all models used an embedding and hidden state size of 48 dimensions. To make the token predictions, each model used a two layer multi-layer perceptron (MLP) with GELU nonlinearities, with a hidden layer size of 4 times the hidden state dimensionality with 50% dropout on the hidden layer. The GRU and LSTM model variants each consisted of a single recurrent cell followed by the output MLP. Unless otherwise stated, the transformer architecture consisted of two layers using Rotary positional encodings (Su et al., 2023). Each model variant used the same learning rate scheduler, which consisted of the original transformer (Vaswani et al., 2017) scheduling of warmup followed by decay. We used 100 warmup steps, a maximum learning rate of 0.001, a minimum of 1e-7, and a decay rate of 0.5. We used a batch size of 128, which caused each epoch to consist of 8 gradient update steps.

#### A.2. MAS (and Associated Variants) Training Details

For each rotation matrix training, we use 10000 intervention samples and 1000 samples for validation and testing. We uniformly sampled corresponding indices upon which to perform interventions, excluding the B, T, and E tokens in the numeric equivalence tasks from possible intervention sample indices. In the Arithmetic task, we used the comma token for Rem Ops and Cumu Val interventions. When intervening upon a state in the demo phase in the numeric equivalence tasks, we uniformly sample 0-3 steps to continue the demo phase before changing the phase by inserting the trigger token. We orthogonalize the matrices,  $Q_i$ , using PyTorch’s orthogonal parametrization with default settings. PyTorch creates the orthogonal matrix as the exponential of a skew symmetric matrix. We train the rotation matrices for 1000 epochs, with a batch size of 512 used for each model index pairing. We only perform experiments considering two models. Each gradient step uses the average gradient over batches of all  $i, j$  pairings. We select the checkpoint with the best validation performance for analysis. We use a learning rate of 0.003 and an Adam optimizer.

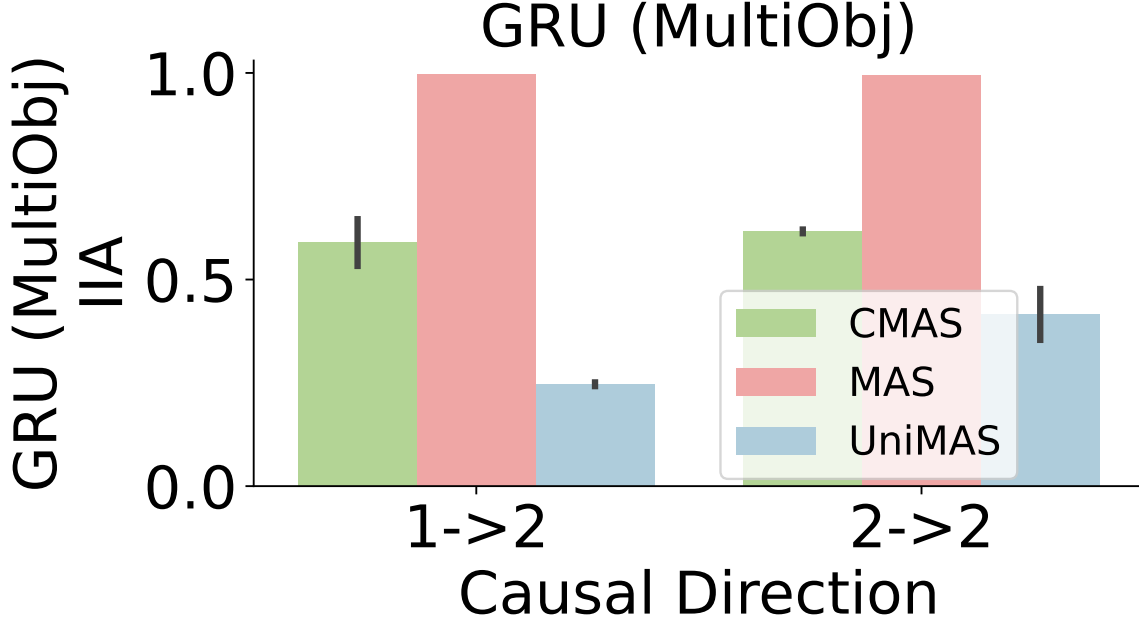


Figure 8: The IIAs in the causally untrained directions for CMAS on the Multi-Object GRU models on the Count variable. The x labels denote the intervention directions where the numbers 1 and 2 denote the model index and the arrow points from the source to the target model. UniMAS and MAS show a lower and upper bound on CMAS performance.

### A.3. RSA Details

We performed RSA on a subsample of a dataset of 15 sampled sequences for each object quantity ranging from 1-20 on the task that each model was trained on for each model. We first ran the models on their respective datasets to collect the latent representations. We sampled 1000 of these latent vectors as the sample representations in a matrix  $M_k \in R^{N \times d_k}$  where  $k$  refers to the model index,  $N$  is the number of latent vectors ( $N = 1000$  in our analyses),  $d_k$  is the dimensionality of a single latent vector for model  $k$ . We then calculated the sample cosine distance matrices (1-cosine similarity) for each model resulting in matrices  $C_k \in R^{N \times N}$ . Lastly we calculated the Spearman’s Rank Correlation Coefficient between the lower triangles of the matrices  $C_1$  and  $C_2$  as the RSA value using python’s SciPy package (Zar, 2005; Kriegeskorte et al., 2008; Virtanen et al., 2020). We resampled the 1000 vectors 10 times and recalculated the RSA score 10 times and report the average over these scores.

### A.4. CKA Details

We performed CKA on a subsample of a dataset of 15 sampled sequences for each object quantity ranging from 1-20 on the task that each model was trained on for each model. We first ran the models on their respective datasets to collect the latent representations. We sampled 1000 of these latent vectors as the sample representations in a matrix  $M_k \in R^{N \times d_k}$  where  $k$  refers to the model index,  $N$  is the number of latent vectors ( $N = 1000$  in our analyses),  $d_k$  is the dimensionality of a single latent vector for model  $k$ . We then normalized the vectors along the sample dimension by subtracting the mean and dividing by the standard deviation (using  $d_k$  means and  $d_k$  standard deviations calculated over 1000 samples). Using these samples we calculated the kernel matrices using cosine similarity to create matrices  $C_k \in R^{N \times N}$ . Using these matrices, we computed the Hilbert-Schmidt Independence Criterion (HSIC) where  $I \in R^{N \times N}$  is the identity and  $J \in R^{N \times N}$  is a matrix of values all equal to 1:

$$H = I - \frac{1}{N}J \quad (10)$$

$$\text{HSIC}(C_1, C_2) = \frac{\text{trace}(C_1 H C_2 H)}{(N-1)^2} \quad (11)$$

and lastly we computed CKA as the following:

$$\text{CKA} = \frac{\text{HSIC}(C_1, C_2)}{\sqrt{\text{HSIC}(C_1, C_1)\text{HSIC}(C_2, C_2)}} \quad (12)$$

(Kornblith et al., 2019). We resampled the 1000 vectors 10 times and recalculated the CKA score 10 times and report the average over these scores.